

Modeling and Simulation of Coupled Cell Proliferation and Regulation in Heterogeneous Tissue

T. I. ZOHDI

Department of Mechanical Engineering, University of California, 6195 Etcheverry Hall, Berkeley, CA 94720-1740, USA

(Received 21 August 2014; accepted 19 November 2014)

Associate Editor Estefanía Peña oversaw the review of this article.

Abstract—The primary objective of this work is to develop a computational framework that efficiently simulates the time-transient proliferation of cellular tissue, with heterogeneous microstructure, utilizing two strongly-coupled conservation laws:

- *Conservation Law 1*: comprises (a) rate of change of cells, (b) cellular migration, (c) cellular proliferation controlled by a cell mitosis regulating chemical, (d) cell apoptosis and
- *Conservation Law 2*: comprises (a) rate of change of the cell mitosis chemical regulator, (b) regulator diffusion, (c) regulator production by cells and (d) regulator decay.

Specifically, a straightforward approach is developed that researchers in the field can easily implement and use as a computationally-efficient tool to study such biological systems. Because multifield coupling is present, a recursive, staggered, temporally-adaptive, Finite Difference Time Domain scheme is developed to resolve the interacting fields. The time-step adaptation allows the numerical scheme to iteratively resolve the changing physical fields by reducing the time-steps during phases of the process when the system is undergoing changes on relatively small time-scales or enlarging the time-steps when the processes are relatively slow. The spatial discretization grids are uniform and dense, and the heterogeneous microstructure, is embedded into the spatial discretization. The regular grid allows one to generate a matrix-free iterative formulation which is amenable to rapid computation and minimal memory requirements, making it ideal for laptop computation. Numerical examples are provided to illustrate the approach.

Address correspondence to T. I. Zohdi, Department of Mechanical Engineering, University of California, 6195 Etcheverry Hall, Berkeley, CA 94720-1740, USA. Electronic mail: zohdi@berkeley.edu

Keywords—Cellular tissue, Proliferation, Regulation, Simulation.

INTRODUCTION

This work is primarily interested in developing a computational framework to enable relatively fast and efficient computation of strongly coupled fields associated with cellular tissue proliferation and regulation. The overall system is broken into two main subsystems, based on two conservation laws:

- *Conservation Law 1*: comprises (a) rate of change of cells, (b) cellular migration, (c) cellular proliferation controlled by a cell mitosis regulating chemical, (d) cell apoptosis and
- *Conservation Law 2*: comprises (a) rate of change of the cell mitosis chemical regulator, (b) regulator diffusion, (c) regulator production by cells and (d) regulator decay.

Throughout the construction of the model, we consider *infinitesimal deformations*, $(\cdot) = \frac{\partial(\cdot)}{\partial t}$. In other words, the domain does not change its shape or geometry with changes in concentration. The “cell” balance (c) per unit volume and a cell mitosis regulating chemical (s) denoted by the normalized concentration of c (cells), in an arbitrary subvolume of material contained within Ω , denoted ω , consists of a concentration (storage) term c , an inward normal migration flux term, $-\mathbf{m} \cdot \mathbf{n}$, a proliferation term, $r(s)$ and a cell apoptosis term, $\tau(c)$, leading to

$$\underbrace{\frac{d}{dt} \int_{\omega} c \, d\omega}_{\text{storage}} = \frac{\partial}{\partial t} \int_{\omega} c \, d\omega \quad (1)$$

$$= - \underbrace{\int_{\partial\omega} \mathbf{m}(c) \cdot \mathbf{n} \, da}_{\text{migration}} + \underbrace{\int_{\omega} r(s) \, d\omega}_{\text{proliferation}} - \underbrace{\int_{\omega} \tau(c) \, d\omega}_{\text{apoptosis}}$$

and simultaneously the balance of a cell mitosis regulating chemical (s)

$$\underbrace{\frac{d}{dt} \int_{\omega} s \, d\omega}_{\text{storage}} = \frac{\partial}{\partial t} \int_{\omega} s \, d\omega \quad (2)$$

$$= - \underbrace{\int_{\partial\omega} \mathbf{f}(s) \cdot \mathbf{n} \, da}_{\text{diffusion}} + \underbrace{\int_{\omega} p(c) \, d\omega}_{\text{production}} - \underbrace{\int_{\omega} \gamma(s) \, d\omega}_{\text{loss}}$$

where s is the cell mitosis regulator concentration, $-\mathbf{f} \cdot \mathbf{n}$ is an inward normal migration flux term, $p(c)$ is a production term and $\gamma(s)$ is a regulator loss term. After using the divergence theorem on the flux terms, since the volume ω is arbitrary, one obtains a diffusion-reaction model in strong form (assuming a Fickian-type law, $\mathbf{m} = -\mathbf{D} \cdot \nabla c$ and $\mathbf{f} = -\mathbf{K} \cdot \nabla s$)

$$\frac{\partial c}{\partial t} = \nabla \cdot \mathbf{D} \cdot \nabla c + r(s) - \tau(c) \quad (3)$$

and simultaneously the balance of a mitosis regulating chemical (s)

$$\frac{\partial s}{\partial t} = \nabla \cdot \mathbf{K} \cdot \nabla s + p(c) - \gamma(s). \quad (4)$$

There is a large body of literature on the construction of the functions $r(s)$, $\tau(c)$, $p(c)$ and $\gamma(s)$ for specific types of problems, such as wound healing. See Murray³³ for an extensive review, with early experimental studies dating back at least to Lindquist²⁸ Van den Brenk,⁴³ Crosson *et al.*,⁶ Zieske *et al.*,⁴⁷ Franz *et al.*⁷ and Sherratt and Murray.⁴⁰ Such a coupled system can represent a variety of biological systems, such as growth in biological scaffolding, proliferation of damaged cellular tissue, *etc.* The modeling of this process has a close similarity to multicomponent diffusion-reaction industrial processes, and we refer the reader to Zohdi.^{48–50}

The objective is to utilize the coupled governing equations (Eqs. (3), (4)) to model the time-transient response of biological material systems, where the media may have complex heterogeneous microstructure. Accordingly, a computational framework that efficiently resolves the strongly coupled time-transient cell and regulator fields that arise is developed. A recursive, staggered, temporally-adaptive, FDTD (Finite Difference Time Domain) scheme is developed that allows the numerical scheme to iteratively resolve the changing physical fields by reducing the time-steps during phases of the process when the system is undergoing changes on relatively small time-scales or to enlarge the time-steps when the processes are relatively slow. The complex heterogeneous microstructure is embedded into a dense regular spatial grid. The

regular grid allows one to generate a matrix-free iterative formulation which is amenable to rapid computation and minimal memory requirements, making it ideal for laptop computation. Numerical examples are provided to illustrate the approach.

Remark Although the approach taken in this work is to directly discretize the system, we remark that there are a number of methods to estimate the overall effective (macroscopic) properties of materials consisting of a matrix, containing a distribution of inhomogeneities, pores or cracks. The literature on this topic is quite extensive, dating back to the early works of Maxwell,³⁰ and Lord Rayleigh.³⁶ For a wide-ranging overview of random heterogeneous media, see Torquato,⁴¹ for more mathematical homogenization aspects, see Jikov *et al.*,²¹ for solid-mechanics issues, see Hashin,¹³ Markov,²⁹ Mura,³² Nemat-Nasser and Hori,³⁴ Huet,¹⁶ for analyses of defect-laden, porous and cracked media, see Kachanov,²² Kachanov, Tsukrov and Shafiro,²³ Kachanov and Sevostianov,²⁴ Sevostianov, Gorbatikh and Kachanov³⁸ Sevostianov and Kachanov³⁹ and for computational aspects, see Zohdi and Wriggers.⁵¹

NUMERICAL SIMULATION OF THE COUPLED SYSTEM

The present section develops a flexible and robust solution strategy to resolve the coupled system. There are two main components to the computational approach:

- Spatio-temporal discretization of the diffusive continuum model,
- Iterative staggering to solve the coupled system, whereby the time-steps are adaptively adjusted to control the error associated with the incomplete resolution of the concentration fields.

Discretization of the c - and s -Fields

The concentration field will require spatial discretization with some type of mesh, for example using a finite difference, finite volume or finite element method.

Temporal Approximation

For the concentration field, we write

$$\frac{\partial c}{\partial t} = \nabla \cdot \mathbf{D} \cdot \nabla c + r(s) - \tau(c) \stackrel{\text{def}}{=} L. \quad (5)$$

We discretize for time $= t + \phi \Delta t$, and using a trapezoidal “ ϕ -scheme” ($0 \leq \phi \leq 1$)

$$c(t + \Delta t) \approx c(t) + \Delta t(\phi L(t + \Delta t) + (1 - \phi)L(t)). \quad (6)$$

Similarly for s ,

$$\frac{\partial s}{\partial t} = \nabla \cdot \mathbf{K} \cdot \nabla s + p(c) - \gamma(s) \stackrel{\text{def}}{=} \mathbf{M}. \quad (7)$$

We discretize for time $t = t + \phi \Delta t$, and using a trapezoidal “ ϕ -scheme” ($0 \leq \phi \leq 1$)

$$s(t + \Delta t) \approx s(t) + \Delta t(\phi \mathbf{M}(t + \Delta t) + (1 - \phi)\mathbf{M}(t)). \quad (8)$$

Spatial Discretization: Spatial Finite Difference finite difference Stencils

The following standard approximations are used:

1. For the first derivative of a primal variable c at (x_1, x_2, x_3) :

$$\frac{\partial c}{\partial x_1} \approx \frac{c(x_1 + \Delta x_1, x_2, x_3) - c(x_1 - \Delta x_1, x_2, x_3)}{2\Delta x_1} \quad (9)$$

2. For the derivative of a flux at (x_1, x_2, x_3) :

$$\begin{aligned} \frac{\partial}{\partial x_1} \left(\mathbf{D} \frac{\partial c}{\partial x_1} \right) &\approx \frac{\left(\mathbf{D} \frac{\partial c}{\partial x_1} \right) \Big|_{x_1 + \frac{\Delta x_1}{2}, x_2, x_3} - \left(\mathbf{D} \frac{\partial c}{\partial x_1} \right) \Big|_{x_1 - \frac{\Delta x_1}{2}, x_2, x_3}}{\Delta x_1} \\ &= \frac{1}{\Delta x_1} \left[\mathbf{D}(x_1 + \frac{\Delta x_1}{2}, x_2, x_3) \right. \\ &\quad \times \left(\frac{c(x_1 + \Delta x_1, x_2, x_3) - c(x_1, x_2, x_3)}{\Delta x_1} \right) \\ &\quad \left. - \frac{1}{\Delta x_1} \left[\mathbf{D}(x_1 - \frac{\Delta x_1}{2}, x_2, x_3) \right. \right. \\ &\quad \left. \left. \times \left(\frac{c(x_1, x_2, x_3) - c(x_1 - \Delta x_1, x_2, x_3)}{\Delta x_1} \right) \right] \right], \end{aligned} \quad (10)$$

where we have used

$$\mathbf{D}(x_1 + \frac{\Delta x_1}{2}, x_2, x_3) \approx \frac{1}{2}(\mathbf{D}(x_1 + \Delta x_1, x_2, x_3) + \mathbf{D}(x_1, x_2, x_3)) \quad (11)$$

and

$$\mathbf{D}(x_1 - \frac{\Delta x_1}{2}, x_2, x_3) \approx \frac{1}{2}(\mathbf{D}(x_1, x_2, x_3) + \mathbf{D}(x_1 - \Delta x_1, x_2, x_3)) \quad (12)$$

Iterative (Implicit) Solution Method

Implicit time-stepping methods, with time step size adaptivity, built on approaches found in Zohdi,^{48–51}

will be used throughout the upcoming analysis. In order to introduce basic concepts, we consider a first order vector-valued differential equation

$$\dot{\mathbf{U}} = \mathbf{F}(\mathbf{U}), \quad (13)$$

which, after being discretized using a trapezoidal “ ϕ -method” ($0 \leq \phi \leq 1$)

$$\mathbf{U}^{L+1} = \mathbf{U}^L + \Delta t(\phi \mathbf{F}(\mathbf{U}^{L+1}) + (1 - \phi)\mathbf{F}(\mathbf{U}^L)), \quad (14)$$

yields the following abstract form

$$\mathcal{A}(\mathbf{U}^{L+1}) = \mathcal{B}. \quad (15)$$

It is convenient to write

$$\mathcal{A}(\mathbf{U}^{L+1}) - \mathcal{B} = \mathcal{G}(\mathbf{U}^{L+1}) - \mathbf{U}^{L+1} + \mathcal{R} = \mathbf{0}, \quad (16)$$

where \mathcal{R} is a remainder term that does not depend on the solution, i.e., $\mathcal{R} \neq \mathcal{R}(\mathbf{U}^{L+1})$. A straightforward iterative scheme can be written as

$$\mathbf{U}^{L+1,K} = \mathcal{G}(\mathbf{U}^{L+1,K-1}) + \mathcal{R}, \quad (17)$$

where $K = 1, 2, 3, \dots$ is the index of iteration within time step $L + 1$. The convergence of such a scheme is dependent on the behavior of \mathcal{G} . Namely, a sufficient condition for convergence is that \mathcal{G} is a contraction mapping for all $\mathbf{U}^{L+1,K}$, $K = 1, 2, 3, \dots$. In order to investigate this further, we define the iteration error as

$$\varpi^{L+1,K} \stackrel{\text{def}}{=} \mathbf{U}^{L+1,K} - \mathbf{U}^{L+1}. \quad (18)$$

A necessary restriction for convergence is iterative self consistency, i.e., the “exact” (discretized) solution must be represented by the scheme

$$\mathcal{G}(\mathbf{U}^{L+1}) + \mathcal{R} = \mathbf{U}^{L+1}. \quad (19)$$

Enforcing this restriction, a sufficient condition for convergence is the existence of a contraction mapping

$$\begin{aligned} \varpi^{L+1,K} &= \|\mathbf{U}^{L+1,K} - \mathbf{U}^{L+1}\| = \|\mathcal{G}(\mathbf{U}^{L+1,K-1}) - \mathcal{G}(\mathbf{U}^{L+1})\| \\ &\leq \eta^{L+1,K} \|\mathbf{U}^{L+1,K-1} - \mathbf{U}^{L+1}\|, \end{aligned} \quad (20)$$

where, if $0 \leq \eta^{L+1,K} < 1$ for each iteration K , then $\varpi^{L+1,K} \rightarrow \mathbf{0}$ for any arbitrary starting value $\mathbf{U}^{L+1,K=0}$, as $K \rightarrow \infty$. This type of contraction condition is sufficient, but not necessary, for convergence. Inserting these approximations into $\dot{\mathbf{U}} = \mathbf{F}(\mathbf{U})$ leads to

$$\mathbf{U}^{L+1,K} \approx \underbrace{\Delta t(\phi \mathbf{F}(\mathbf{U}^{L+1,K-1}))}_{\mathcal{G}(\mathbf{U}^{L+1,K-1})} + \underbrace{\Delta t(1 - \phi)\mathbf{F}(\mathbf{U}^L) + \mathbf{U}^L}_{\mathcal{R}}, \quad (21)$$

whose contraction constant is scaled by $\eta \propto \phi \Delta t$. Therefore, if convergence is slow within a time step, the

time step size, which is adjustable, can be reduced by an appropriate amount to increase the rate of convergence. Decreasing the time step size improves the convergence, however, we want to simultaneously maximize the time-step sizes to decrease overall computing time, while still meeting an error tolerance on the numerical solution's accuracy. In order to achieve this goal, we follow an approach found in Zohdi⁴⁸ originally developed for continuum thermo-chemical multifield problems in which one first approximates

$$\eta^{L+1,K} \approx S(\Delta t)^p \quad (22)$$

(S is a constant) and secondly one assumes the error within an iteration to behave according to

$$(S(\Delta t)^p)^K \varpi^{L+1,0} = \varpi^{L+1,K}, \quad (23)$$

$K = 1, 2, \dots$, where $\varpi^{L+1,0}$ is the initial norm of the iterative error and S is intrinsic to the system.¹ Our goal is to meet an error tolerance in exactly a preset number of iterations. To this end, one writes

$$(S(\Delta t_{tol})^p)^{K_d} \varpi^{L+1,0} = C_{tol}, \quad (24)$$

where C_{tol} is a (coupling) tolerance and where K_d is the number of desired iterations.² If the error tolerance is not met in the desired number of iterations, the contraction constant $\eta^{L+1,K}$ is too large. Accordingly, one can solve for a new smaller step size, under the assumption that S is constant,

$$\Delta t_{tol} = \Delta t \left(\frac{\left(\frac{C_{tol}}{\varpi^{L+1,0}} \right)^{\frac{1}{pK_d}}}{\left(\frac{\varpi^{L+1,K}}{\varpi^{L+1,0}} \right)^{\frac{1}{pK}}} \right). \quad (25)$$

The assumption that S is constant is not critical, since the time steps are to be recursively refined and unrefined throughout the simulation. Clearly, the expression in Eq. (25) can also be used for time step enlargement, if convergence is met in less than K_d iterations.³ Specifically, the solution steps are, within a time-step:

- (1): Start a global fixed iteration (set $i = 1, \dots, N_n$ (node counter) and $K = 0$ (iteration counter))
- (2): If $i > N_n$ then go to (4)
- (3): If $i \leq N_n$ then:
 - (a) Compute the concentration $c_i^{L+1,K}$
 - (b) Go to (2) for the next node ($i = i + 1$)

- (4): Repeat steps 1-3 for the nodes, $i = 1, \dots, N_n$.
- (5): Measure error (normalized) quantities (where w_c is a weight on the cell contribution and w_s is a weight on the regulator contribution)
 - (a) $\varpi^{L+1,K} \stackrel{def}{=} w_c \frac{\sum_{i=1}^{N_n} \|c_i^{L+1,K} - c_i^{L+1,K-1}\|}{\sum_{i=1}^{N_p} \|s_i^{L+1,K} - s_i^{L+1,K-1}\|} + w_s \frac{\sum_{i=1}^{N_n} \|c_i^{L+1,K}\|}{\sum_{i=1}^{N_p} \|s_i^{L+1,K}\|}$
 - (b) $Z_K \stackrel{def}{=} \frac{\varpi^{L+1,K}}{TOL}$ where TOL is an error tolerance.
 - (c) $\Lambda_K \stackrel{def}{=} \left(\frac{\left(\frac{TOL}{\varpi^{L+1,0}} \right)^{\frac{1}{pK_d}}}{\left(\frac{\varpi^{L+1,K}}{\varpi^{L+1,0}} \right)^{\frac{1}{pK}}} \right)$.
- (6): If the tolerance is met: $Z_K \leq 1$ and $K < K_d$ then
 - (a) Increment time: $t = t + \Delta t$
 - (b) Construct the next time step: $(\Delta t)^{new} = \Lambda_K (\Delta t)^{old}$,
 - (c) Select the minimum size: $\Delta t = MIN((\Delta t)^{lim}, (\Delta t)^{new})$ and go to (1)
- (7): If the tolerance is not met: $Z_K > 1$ and $K < K_d$ then
 - (a) Update the iteration counter: $K = K + 1$
 - (b) Reset the node counter: $i = 1$
 - (c) Go to (2)
- (8): If the tolerance is not met ($Z_K > 1$) and $K = K_d$ then
 - (a) Construct a new time step: $(\Delta t)^{new} = \Lambda_K (\Delta t)^{old}$
 - (b) Restart at time t and go to (1)

Time-step size adaptivity is critical, since the system's dynamics can dramatically change over the course of time, possibly requiring quite different time step sizes to control the iterative error. However, to maintain the accuracy of the time-stepping scheme, one must respect an upper bound dictated by the discretization error, i.e., $\Delta t \leq \Delta t^{lim}$. Note that in step (5), Λ_K may enlarge the time-step if the error is lower than the preset tolerance. At a given time, once the process is complete, the time is incremented forward and the process is repeated. The overall goal is to deliver solutions where the iterative error is controlled and the temporal discretization accuracy dictates the upper limit on the time step size (Δt^{lim}). Clearly, there are various combinations of solution methods that one can choose from. For example, for the overall field coupling, one may choose implicit or explicit staggering and within the staggering process, either implicit ($0 < \phi \leq 1$) or explicit time-stepping ($\phi = 0$), and, in the case of implicit time-stepping, iterative or direct solvers. Furthermore, one could employ internal iterations for each field equation, then update, more sophisticated metrics for certain components of the

¹For the class of problems under consideration, due to the quadratic dependency on Δt , $p \approx 1$.

²Typically, K_d is chosen to be between five to ten iterations, although this is problem and analyst dependent.

³At the implementation level, since the exact solution is unknown, the following relative error term is used, $\varpi^{L+1,K} \stackrel{def}{=} \mathbf{U}^{L+1,K} - \mathbf{U}^{L+1,K-1}$.

error, *etc.* For example, we utilized an error measure that used the concentrations at the nodes of the Finite Difference grid, but other metrics are certainly possible. For details see Zohdi.^{48–51}

Remark 1 Because the internal system solvers within the staggering scheme are also iterative and use the previously converged solution as their starting value to solve the system of equations, a field that is relatively insensitive at given stage of the simulation will converge in very few internal iterations (perhaps even one). Staggering schemes are widely used in the computational mechanics literature, dating back, at least, to Zienkiewicz⁴⁵ and Zienkiewicz *et al.*⁴⁶ For in depth overviews, see the works of Lewis and Schrefler (Lewis *et al.*²⁶ and Lewis and Schrefler²⁷) and a series of works by Schrefler and collaborators: Schrefler,³⁷ Turska and Schrefler,⁴² Bianco *et al.*³ and Wang and Schrefler.⁴⁴

Remark 2 At the length-scales of interest, it is questionable whether the ideas of a sharp material interface are justified. Accordingly, we simulated the system with and without Laplacian smoothing, whereby one smooths the material data by post-processing the material data, node by node, to produce a smoother material representation, for example, for the cell diffusivity, $\hat{\mathbf{D}}$

$$\begin{aligned} \nabla_{\mathbf{x}}^2 \mathbf{D} = \mathbf{0} \Rightarrow \hat{\mathbf{D}}_{i,j,k} = \frac{1}{6} (\mathbf{D}_{i+1,j,k} + \mathbf{D}_{i-1,j,k} + \mathbf{D}_{i,j+1,k} \\ + \mathbf{D}_{i,j-1,k} + \mathbf{D}_{i,j,k+1} + \mathbf{D}_{i,j,k-1}). \end{aligned} \quad (26)$$

The same was done for \mathbf{K} by enforcing $\nabla_{\mathbf{x}}^2 \mathbf{K} = \mathbf{0}$. The simulations were run with and without data smoothing, with the results being negligibly different for sufficiently fine meshes (Fig. 1).

NUMERICAL EXAMPLES

As an example, we consider a cubical domain with an initial interior concentration of zero cells and zero regulator. We inject both cells and regulator at a given location at the top (Fig. 2). The injection site is elliptical and has controlled concentration of both cells and regulator over time. The boundary conditions for the cells and regulator were held to be zero, other than at the injection site. We considered two scenarios: (a) a benchmark domain where the medium is homogeneous and (b) a heterogeneous domain where the medium has a microstructure comprised of randomly distributed spheres (occupying approximately 25 % volume fraction) in a homogeneous matrix. The following

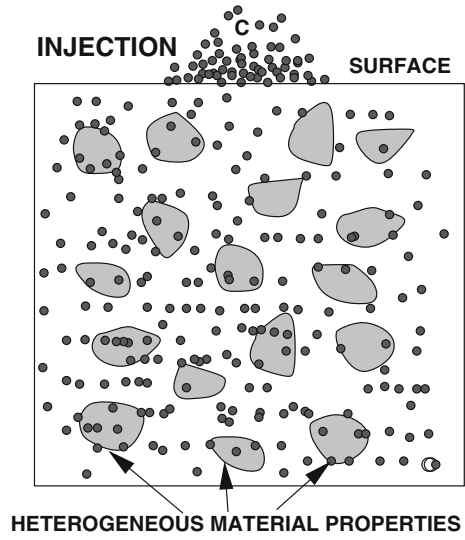


FIGURE 1. The model problem with heterogeneous microstructure. This could represent scaffolding or simply heterogeneous tissue. The injection site is given high concentration of cells and regulator, for example modeling an injection of topological additive.

parameters were used (with standard metric units used throughout):

- size of the domain was $0.01 \times 0.01 \times 0.01 \text{ m}$,
- injection site, a controlled cell concentration $c(t) = c_0 e^{at}$, $c_0 = 1$, $a = 0.01$,
- injection site, a controlled regulator concentration $s(t) = s_0 e^{at}$, $s_0 = 1$, $a = 0.01$,
- injection site was $0.005 \times 0.00125 \text{ m}$ (elliptical cross-section) and 0.0025 m deep,
- total simulation time was $T = 20 \text{ s}$,
- cell proliferation term, $r(s) = +\hat{r}s$, with a different \hat{r} for each material phase,
- cell apoptosis term, $\tau(c) = -\hat{\tau}c$, with a different $\hat{\tau}$ for each material phase,
- regulator production term, $p(c) = +\hat{p}c$, with a different \hat{p} for each material phase,
- regulator loss term, $\gamma(s) = -\hat{\gamma}s$, with a different $\hat{\gamma}$ for each material phase,
- homogeneous case, $\hat{r}_o = 20$, $\hat{r}_{1R} = \frac{\hat{r}_1}{\hat{r}_o} = 10$,
- homogeneous case, $\hat{\tau}_o = 0.1$, $\hat{\tau}_{1R} = \frac{\hat{\tau}_1}{\hat{\tau}_o} = 10$,
- homogeneous case, $\hat{p}_o = 0.001$, $\hat{p}_{1R} = \frac{\hat{p}_1}{\hat{p}_o} = 100$,
- homogeneous case, $\hat{\gamma}_o = 0.1$, $\hat{\gamma}_{1R} = \frac{\hat{\gamma}_1}{\hat{\gamma}_o} = 100$,
- homogeneous case, $\hat{\mathbf{D}} = D\mathbf{1}$, $D = 10^{-6}$,
- homogeneous case, $\hat{\mathbf{K}} = K\mathbf{1}$, $K = 10^{-7}$,
- heterogeneous case, $\hat{r}_o = 20$, $\hat{r}_{1R} = \frac{\hat{r}_1}{\hat{r}_o} = 10$, $\hat{r}_{2R} = \frac{\hat{r}_2}{\hat{r}_o} = 1$,
- heterogeneous case, $\hat{\tau}_o = 0.1$, $\hat{\tau}_{1R} = \frac{\hat{\tau}_1}{\hat{\tau}_o} = 10$, $\hat{\tau}_{2R} = \frac{\hat{\tau}_2}{\hat{\tau}_o} = 1$,
- heterogeneous case, $\hat{p}_o = 0.001$, $\hat{p}_{1R} = \frac{\hat{p}_1}{\hat{p}_o} = 100$, $\hat{p}_{2R} = \frac{\hat{p}_2}{\hat{p}_o} = 1$,

- heterogeneous case, $\hat{\gamma}_o = 0.1$, $\hat{\gamma}_{1R} = \frac{\hat{\gamma}_1}{\hat{\gamma}_o} = 100$, $\hat{\gamma}_{2R} = \frac{\hat{\gamma}_2}{\hat{\gamma}_o} = 1$,
- heterogeneous case, $\mathbf{D}_1 = D_1 \mathbf{1}$, $D_1 = 10^{-6}$ and $\mathbf{D}_2 = D_2 \mathbf{1}$, $D_2 = 10^{-7}$,

- heterogeneous case, $\mathbf{K}_1 = K_1 \mathbf{1}$, $K_1 = 10^{-7}$ and $\mathbf{K}_2 = K_2 \mathbf{1}$, $K_2 = 10^{-8}$.

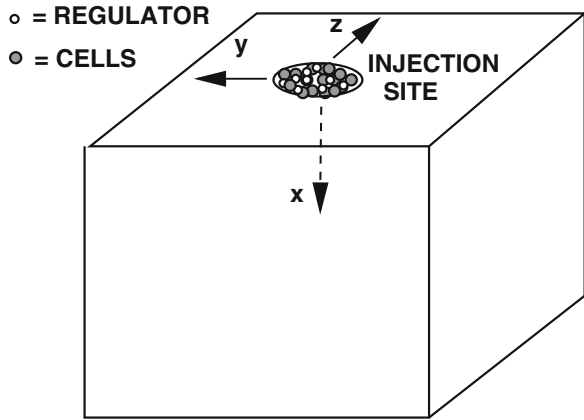


FIGURE 2. The cells and regulator are injected at the location indicated. The boundary and initial conditions are zero for both fields (other than at the injection site).

The time steps were initially started to be quite small in order to allow the system to evolve the time step size during the beginning of the simulation. A trapezoidal time stepping parameter of $\phi = 0.5$ was chosen. In this case, we started the time-step size at 0.001 s and allowed it to be enlarged up to 20 times that size, if the algorithm and error estimates warranted it (which was the case in the examples given). During the computations with the heterogeneous media, the spatial discretization meshes were repeatedly refined until the solutions did not exhibit any more sensitivity to further refinement of the grid-spacing. We started with meshes such as a $21 \times 21 \times 21$ mesh, arising from having a cubical mesh with 10 nodes from the centerline plane of symmetry and one node in the middle, and then repeatedly refined in the following sequential manner:

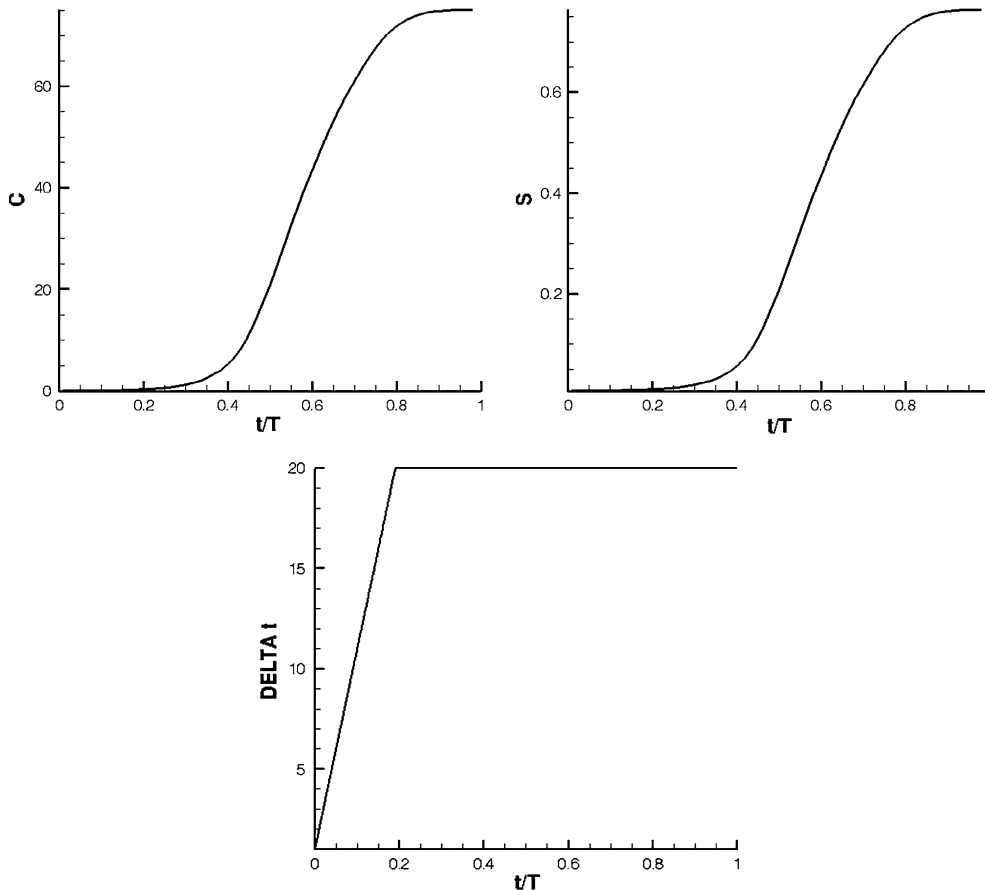


FIGURE 3. Without microstructure: from left to right and top to bottom: (a) The average concentration of cells over time. (b) The average concentration of regulator over time. (c) The evolution of the time-step size over time.

Modeling and Simulation of Coupled Cell Proliferation

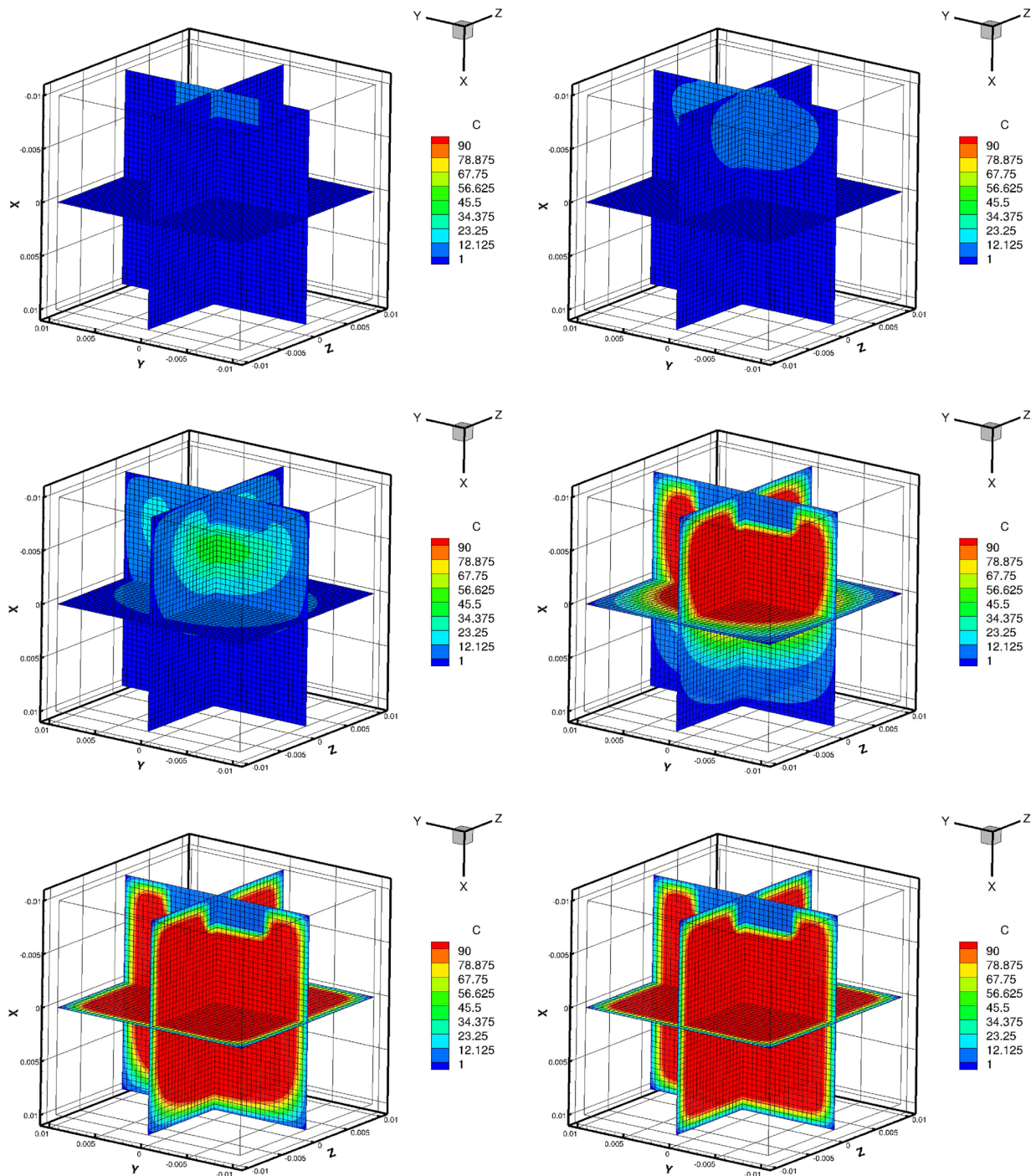


FIGURE 4. Without microstructure: from left to right and top to bottom: Cell concentration (c) and growth from an injection at the surface. Please note that the color scale is different than that for the regulator concentration (s).

1. **Mesh # 1:** a $21 \times 21 \times 21$ mesh, which has 9261 *degrees of freedom* per field, for a total of 18,522 *degrees of freedom*,
2. **Mesh # 2:** a $41 \times 41 \times 41$ mesh, which has 68,921 *degrees of freedom* per field, for a total of 137,842 *degrees of freedom*,

3. **Mesh # 3:** a $61 \times 61 \times 61$ mesh which has 226,981 *degrees of freedom* per field, for a total of 453,962 *degrees of freedom*, etc.

Approximately between a 41-level and a 61-level mesh, the results stabilized, indicating that the results are essentially free of any appreciable numerical error. As

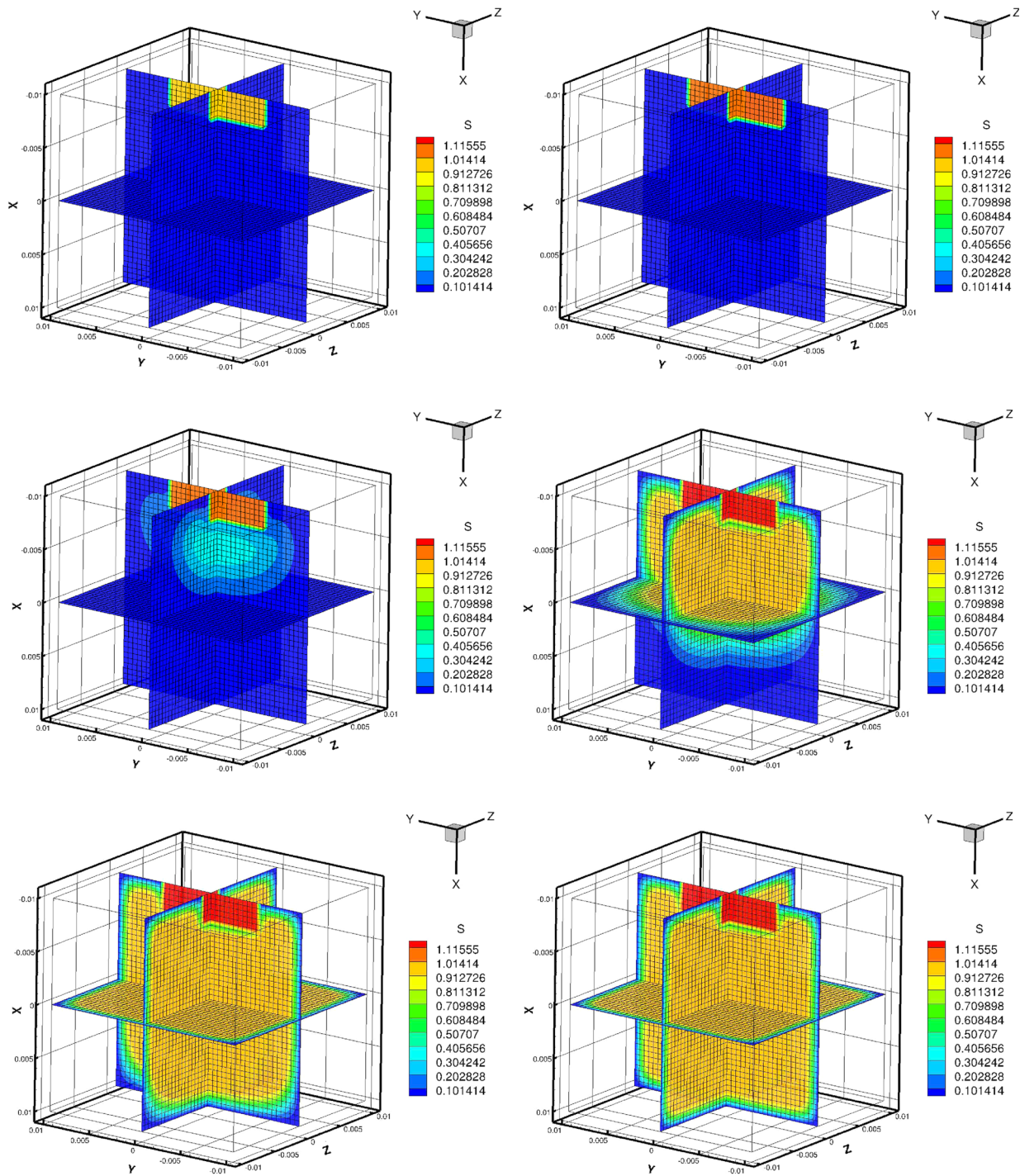


FIGURE 5. Without microstructure: from left to right and top to bottom: regulator (s) concentration and growth from an injection at the surface. Please note that the color scale is different than that for the cell concentration (c).

a type of initial benchmark problem, Case 1 illustrates the solution in a homogeneous (benchmark) medium. Figure 3 depicts (a) The average concentration of cells over time and (b) The average concentration of regulator over time. The solution exhibits a symmetry, due to the uniform microstructure. Figure 4 shows

cross-sections of the concentration of cells domain over time, while Fig. 5 illustrates cross-sections of the concentration of regulator domain over time. Case 2 illustrated the solution in a heterogeneous medium (25 % volume fraction of randomly distributed spherical inclusions), where the (lower-permeability) properties

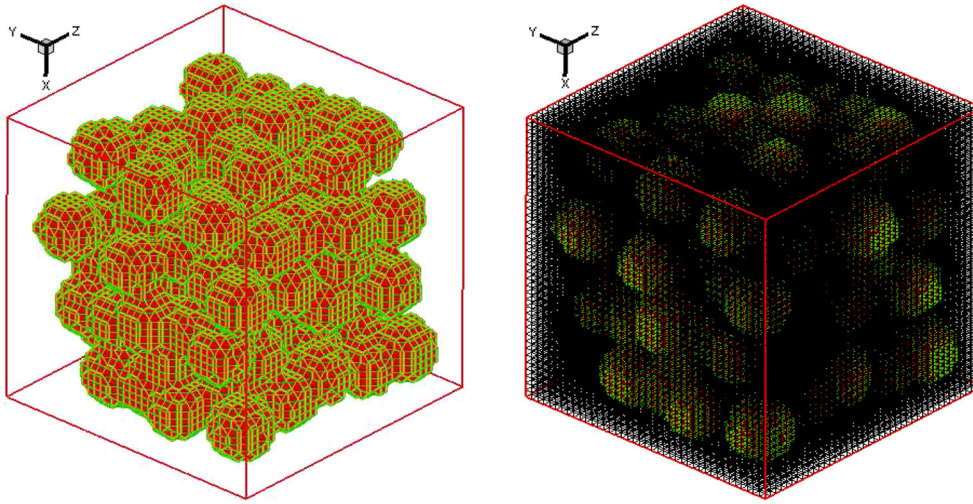


FIGURE 6. With microstructure: (a) The morphology of the microstructure and (b) The morphology of the microstructure and mesh.

were given previously in the itemized list. Figure 6 illustrates the morphology of the microstructure as resolved by the grid. Figure 7 depicts (a) The average concentration of cells over time, (b) The average concentration of regulator over time and (c) The evolution of the time-step size over time. Figure 8 shows cross-sections of the concentration of cells domain over time. Figure 9 illustrates cross-sections of the concentration of regulator domain over time. Clearly, the lower permeability microstructure impedes the process, relative to the uniform microstructure-free material, resulting in a much more complex evolution of both the cell and regulator concentrations. It is important to note that for the homogeneous case, the fields did achieve steady state values in the time period chosen. In order to make comparisons between the homogeneous and heterogeneous media cases, the heterogeneous media case was simulated for the same time duration as the homogeneous one. For the heterogeneous case, the c and s fields do not achieve steady state in the same time period as the homogeneous case. The computations are designed so that they take a few minutes on a standard laptop. The selected parameter choices were provided to illustrate the overall working on the model, and a wide variety of parameter choices are possible, depending on the application. This is discussed further next.

DISCUSSION AND SUMMARY

In summary, the purpose of this paper was to present a flexible computational modeling framework approach, which can be numerically implemented with minimal effort by researchers interested in the simula-

tion of systems comprised of the growth of cells coupled to a cell mitosis regulator. In the examples provided, the time steps were set purposely small at the start to allow the system to determine the time step size. The spatial discretization grids were uniform and dense, and the heterogeneous microstructure, was embedded into spatial discretization. The regular grid allows one to generate a matrix-free iterative formulation which is amenable to rapid computation and minimal memory requirements, making it ideal for laptop computation. Numerical examples were provided to illustrate the approach for a test set of parameters. The framework is flexible enough to allow researchers to input virtually any type of cell and cell regulator interaction. However, in the present formulation, notably absent are the effects of deformation and stress in the system. At a minimum, this would require a third field equation governing the balance of linear momentum, $\nabla_x \cdot \boldsymbol{\sigma} + \mathbf{f} = \rho \dot{\mathbf{v}}$, where $\boldsymbol{\sigma}$ is the Cauchy stress, \mathbf{f} are the body forces, ρ is the density and \mathbf{v} is the velocity, in addition to constitutive laws for soft tissue (see the extensive works of Fung,⁸ Holzapfel,¹⁴ or Humphrey,¹⁸). At finite deformations, the previous conservation laws can be generativated in the following manner:

$$\begin{aligned}
 \frac{d}{dt} \int_{\omega} c \, d\omega &= \frac{d}{dt} \int_{\omega_o} c J \, d\omega_o = \int_{\omega_o} \left(\frac{dc}{dt} J + c \frac{dJ}{dt} \right) d\omega_o \\
 &= \int_{\omega_o} \left(\frac{dc}{dt} J + c J \nabla_x \cdot \mathbf{v} \right) d\omega_o \\
 &= \int_{\omega} \left(\frac{\partial c}{\partial t} + \mathbf{v} \cdot \nabla_x c + c \nabla_x \cdot \mathbf{v} \right) d\omega = \int_{\omega} \left(\frac{\partial c}{\partial t} + \nabla_x \cdot (c\mathbf{v}) \right) d\omega
 \end{aligned} \tag{27}$$

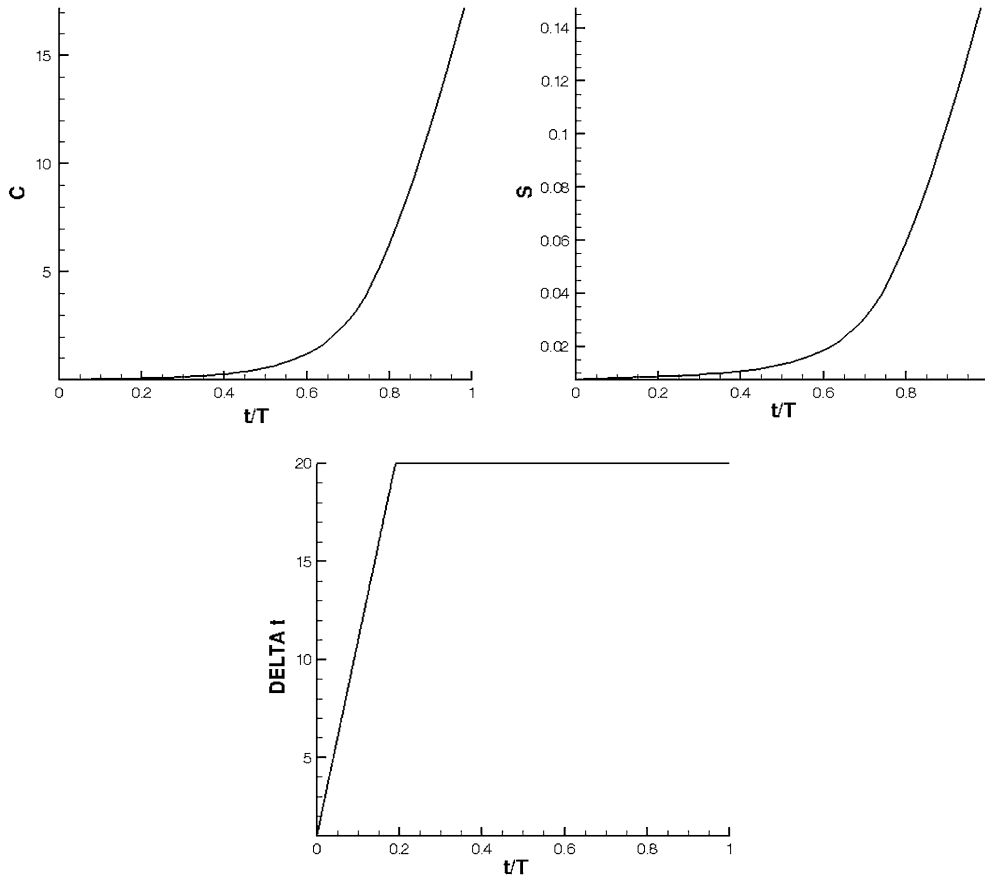


FIGURE 7. With microstructure: from left to right and top to bottom: (a) The average concentration of cells over time. (b) The average concentration of regulator over time. (c) The evolution of the time-step size over time.

thus

$$\frac{\partial c}{\partial t} + \nabla_x \cdot (c\mathbf{v}) = \nabla \cdot \mathbf{D} \cdot \nabla c + r(s) - \tau(c). \quad (28)$$

and

$$\frac{\partial s}{\partial t} + \nabla_x \cdot (s\mathbf{v}) = \nabla \cdot \mathbf{K} \cdot \nabla s + p(c) - \gamma(s). \quad (29)$$

Incorporation of the deformation effects is currently under investigation by the author. Clearly, specific material data is needed for tissue. In this regard, we again refer the reader to Murray³³ for an extensive review, with early experimental studies dating back at least to Lindquist²⁸ Van den Brenk,⁴³ Crosson *et al.*,⁶ Zieske *et al.*,⁴⁷ Franz *et al.*⁷ and Sherratt and Murray.⁴⁰ Generally, because the distribution of water, biological fluids and chemical species within such tissue are dependent on the deformation of the solid, coupled multifield computations are necessary to realistically

simulate such systems. *For example*, in many models of muscle tissue, it is usually assumed that the response depends on the concentration of a mobile chemical species present, for example, intracellular calcium Ca^{2+} , and U is the stretch along the muscle fiber, relative to a reference sarcomere length. A basic form suggested is $\sigma = \sigma(Ca^{2+}, U)$, where σ is the total Cauchy stress (active and passive), which combines the mechanical (passive) contribution and the actively generated muscle tension. We refer the reader to Rachev and Hayashi,³⁵ Humphrey,^{18,19} Klepach *et al.*²⁵ and Ambrosi *et al.*¹ for reviews. Finally, we comment that the technique used in this paper is clearly not the only approach to describe tissue regeneration. There are other approaches used in the literature to study tissue regeneration. The literature in this field is quite extensive, for example with applications to bone, see Geris *et al.*,¹¹ Isaksson *et al.*,²⁰ Gomez-Benito *et al.*,¹² Bailon and van der Meulen,² Checa *et al.*⁵ and Carlier *et al.*⁴

Modeling and Simulation of Coupled Cell Proliferation

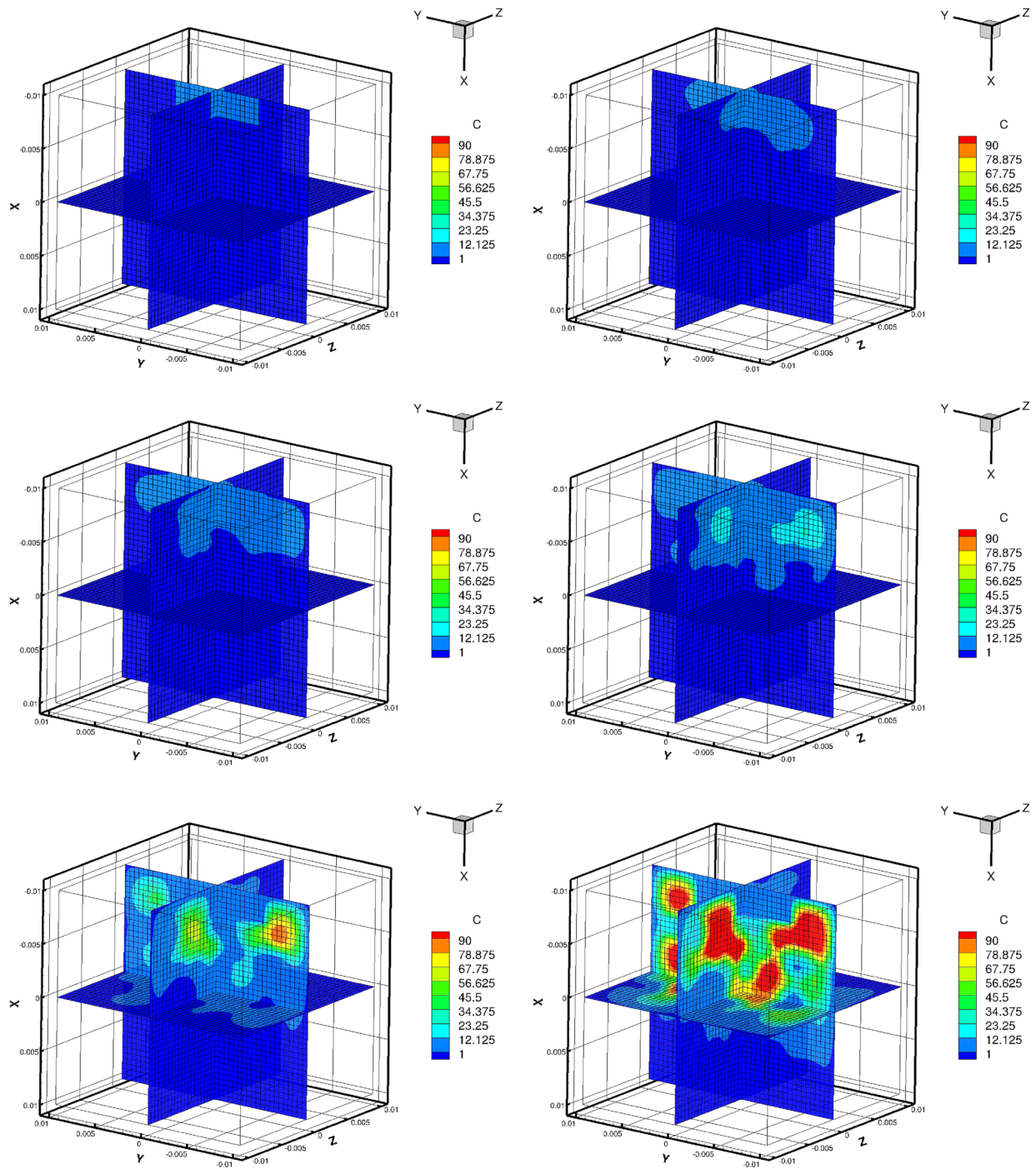


FIGURE 8. With microstructure: from left to right and top to bottom: Cell concentration (c) and growth from an injection at the surface. Please note that the color scale is different than that for the regulator concentration (s).

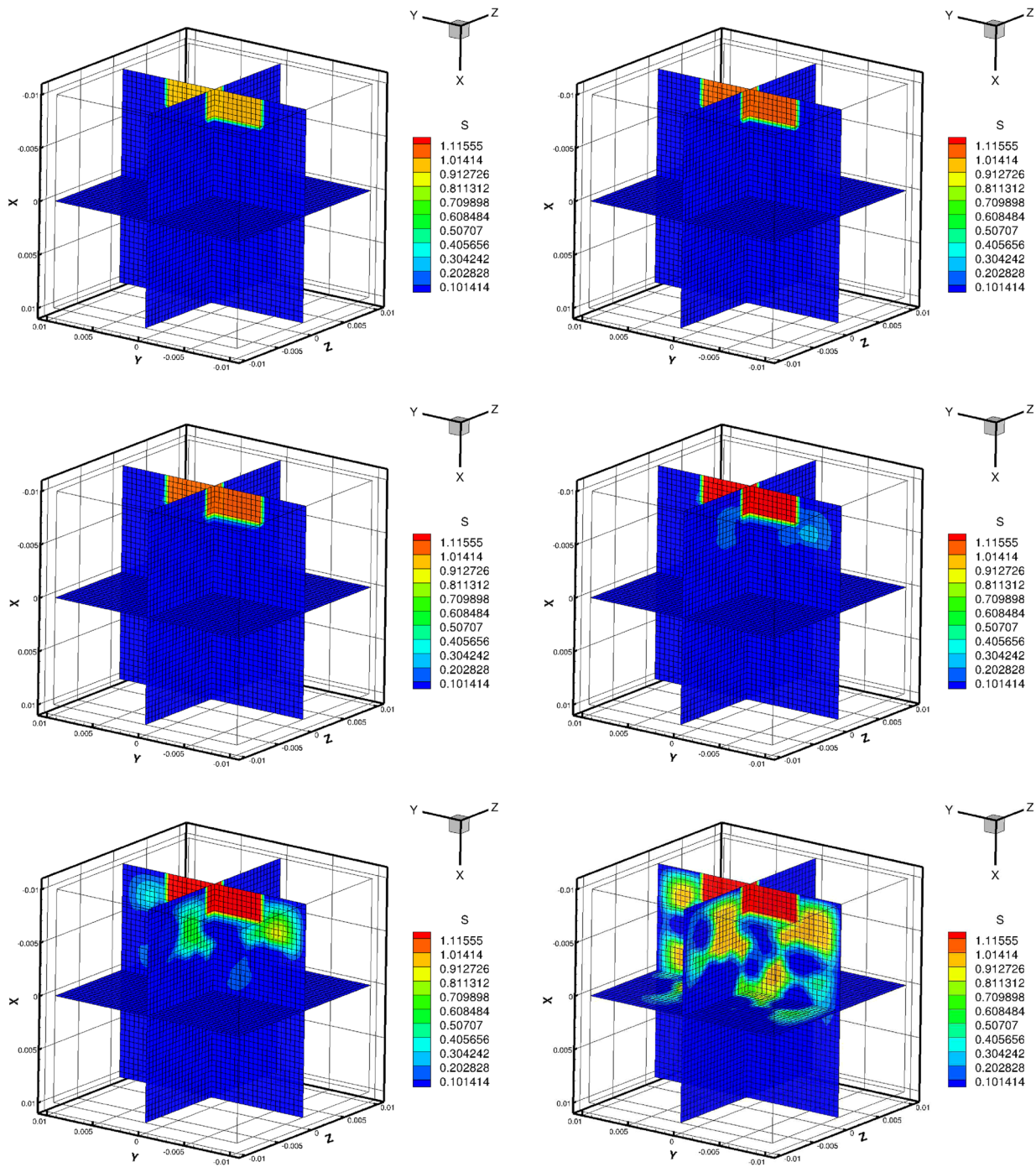


FIGURE 9. With microstructure: from left to right and top to bottom: Regulator (s) concentration and growth from an injection at the surface. Please note that the color scale is different than that for the cell concentration (c).

REFERENCES

¹ Ambrosi, D., Ateshian, G. A., Arruda, E. M., Cowin, S. C., Dumais, J., Goriely, A., Holzapfel, G. A., Humphrey, J. D., Kemkemer, R., Kuhl, E., Olberding, J. E., Taber, L. A. and Garikipati, K. Perspectives on biological growth and remodeling. *J. Mech. Phys. Solids* 59:863–883, 2011.

² Bailon-Plaza, A., and M. van der Meulen. Beneficial effects of moderate, early loading and adverse effects of delayed

or excessive loading on bone healing. *J. Biomech.* 36(8):1069–1077, 2003.

³ Bianco, M., G. Bilardi, F. Pesavento, G. Pucci, and B. A. Schrefler. A frontal solver tuned for fully coupled non-linear hygro-thermo-mechanical problems. *Int. J. Numer. Methods Eng.* 57:1801–1818, 2003.

⁴ Carlier, A., L. Geris, K. Bentley, G. Carmeliet, P. Carmeliet, and H. Van Oosterwyck. (2012). MOSAIC: a multiscale model of osteogenesis and sprouting angiogen-

- esis with lateral inhibition of endothelial cells. *PLoS Comput. Biol.* 8(10), 2012.
- ⁵Checa, S., P. J. Prendergast, and G. N. Duda. Inter-species investigation of the mechano-regulation of bone healing: comparison of secondary bone healing in sheep and rat. *J. Biomech.* 44:1237–1245, 2011.
 - ⁶Crosson, C. E., S. D. Klyce, and R. W. Beuerman. Epithelial wound closure in rabbit cornea wounds invest. *Ophthalmol Vis. Sci.* 27:464–473, 1986.
 - ⁷Franz, J. M., B. M. Dupuy, H. E. Kaufman, and R. W. Beuerman. The effects of collagen shields on epithelial wound healing in rabbits. *Am. J. Ophthalmol.* 108:524–528, 1989.
 - ⁸Fung, Y. C. Elasticity of soft tissues in simple elongation. *Am. J. Physiol.* 28:1532–1544, 1967.
 - ⁹Fung, Y. C. Biorheology of soft tissues. *Biorheology* 10:139–155, 1973.
 - ¹⁰Fung, Y. C. (1983). On the foundations of biomechanics. *ASME J. Appl. Mech.* 50, 1003–1009.
 - ¹¹Geris, L., K. Van damme, I. Naert, J. Van der Slotena, J. Duyck, and H. Van Oosterwyck. Application of mechano-regulatory models to simulate peri-implant tissue formation in an in vivo bone chamber. *J. Biomech.* 41:145–154.
 - ¹²Gomez-Benito, M. J., J. M. Garcia-Aznar, J. H. Kuiper, and M. Doblare. Influence of fracture gap size on the pattern of long bone healing: a computational study. *J. Theor. Biol.* 235:105–119, 2005.
 - ¹³Hashin, Z. Analysis of composite materials: a survey. *ASME J. Appl. Mech.* 50:481–505, 1983.
 - ¹⁴Holzapfel, G. A. Biomechanics of soft tissue. The handbook of materials behavior models. Volume III, Multiphysics behaviors, Chap. 10, Composite Media, Biomaterials, edited by J. Lemaitre. Boston: Academic Press, pp. 1049–1063, 2001.
 - ¹⁵Holzapfel, G. A., and R. W. Ogden. Biomechanical Modeling at the Molecular, Cellular and Tissue Levels. Springer-Verlag, 2009.
 - ¹⁶Huet, C. Universal conditions for assimilation of a heterogeneous material to an effective medium. *Mech. Res. Commun.* 9 (3), 165–170, 1982.
 - ¹⁷Huet, C. On the definition and experimental determination of effective constitutive equations for heterogeneous materials. *Mech. Res. Commun.* 11 (3), 195–200, 1984.
 - ¹⁸Humphrey, J. D. Cardiovascular Solid Mechanics. Cells, Tissues, and Organs. New York: Springer-Verlag, 2002.
 - ¹⁹Humphrey, J. D. Continuum biomechanics of soft biological tissues. *Proc. R. Soc.* 459(2029):3–46, 2003.
 - ²⁰Isaksson, H., C. van Donkelaar, and K. Ito. Sensitivity of tissue differentiation and bone healing predictions to tissue properties. *J. Biomech.* 26, 555–564, 2009.
 - ²¹Jikov, V. V., S. M. Kozlov, and O. A. Olenik. Homogenization of Differential Operators and Integral Functionals. Springer-Verlag, 1994.
 - ²²Kachanov, M. Elastic solids with many cracks and related problems. *Advance Applied Mechanics*, vol. 30. New York: Academic Press, 1993, p. 259.
 - ²³Kachanov, M., I. Tsukrov, and B. Shafiro. Effective moduli of solids with cavities of various shapes. *Appl. Mech. Rev.* 47:S151–S174, 1994.
 - ²⁴Kachanov, M., and I. Sevostianov. On the quantitative characterization of microstructures and effective properties. *Int. J. Solids Struct.* 42, 309–336, 2005.
 - ²⁵Klepach, D., L. C. Lee, J. Wenk, M. Ratcliffe, T. I. Zohdi, J. Navia, G. Kassab, E. Kuhl, and J. M. Guccione. Growth and remodeling of the left ventricle: a case study of myocardial infarction and surgical ventricular restoration. *Mech. Res. Commun.* 42:134–141, 2012.
 - ²⁶Lewis, R. W., B. A. Schrefler, and L. Simoni. Coupling versus uncoupling in soil consolidation. *Int. J. Numer. Anal. Methods. Geomech* 15:533–548.
 - ²⁷Lewis, R. W., and B. A. Schrefler. The Finite Element Method in the Static and Dynamic Deformation and Consolidation of Porous Media. 2nd edn. Wiley Press, 1998.
 - ²⁸Lindquist, G. The healing of skin defects: an experimental study of the white rat. *Acta Chir. Scand.* 94:1–163, Supplement 107, 1946.
 - ²⁹Markov, K. Z. Elementary micromechanics of heterogeneous media. In: *Heterogeneous Media: Micromechanics Modeling Methods and Simulations*, edited by K. Z. Markov, and L. Preziosi. Boston: Birkhauser, 2000, pp. 1–162.
 - ³⁰Maxwell, J. C. On the dynamical theory of gases. *Philos. Trans. Soc. Lond.* 157:49, 1867.
 - ³¹Maxwell, J. C. A Treatise on Electricity and Magnetism. 3rd. edn. Oxford: Clarendon Press, 1873.
 - ³²Mura, T. *Micromechanics of Defects in Solids*, 2nd edn. Kluwer Academic Publishers, 1993.
 - ³³Murray, J. D. *Mathematical Biology*, 3rd edn. Springer Verlag, 2004.
 - ³⁴Nemat-Nasser, S., and M. Hori. *Micromechanics: Overall Properties of Heterogeneous Solids*. 2nd edn. Amsterdam: Elsevier, 1999.
 - ³⁵Rachev, A., and K. Hayashi. Theoretical study of the effects of vascular smooth muscle contraction on strain and stress distributions in arteries. *Ann. Biomed. Eng.* 27:459–468, 1999.
 - ³⁶Rayleigh, J. W. On the influence of obstacles arranged in rectangular order upon properties of a medium. *Philos. Mag.* 32:481–491, 1892.
 - ³⁷Schrefler, B. A. A partitioned solution procedure for geothermal reservoir analysis. *Commun. Appl. Numer. Methods.* 1:53–56, 1985.
 - ³⁸Sevostianov, I., L. Gorbatikh, and M. Kachanov. Recovery of information of porous/microcracked materials from the effective elastic/conductive properties. *Mater. Sci. Eng. A.* 318:1–14, 2001.
 - ³⁹Sevostianov, I., and M. Kachanov. Connections between elastic and conductive properties of heterogeneous materials. *Adv. Appl. Mech.* 42:69–253, 2008.
 - ⁴⁰Sherratt, J. A., and J. D. Murray. Models of epiderma wound healing. *Proc. R. Soc. Lond. B.* 241:29–36, 1990.
 - ⁴¹Torquato, S. *Random Heterogeneous Materials: Microstructure and Macroscopic Properties*. New York: Springer-Verlag, 2002.
 - ⁴²Turska, E., and B. A. Schrefler. On Consistency, Stability and Convergence of Staggered Solution Procedures. *Rend. Mat. acc. Rome: Lincei, S. 9, v. 5*, pp. 265–271.
 - ⁴³Van den Brenk, H. A. S Studies in restorative growth processes in mammalian wound healing. *Br. J. Surg.* 43:525–550, 1956.
 - ⁴⁴Wang, X., and B. A. Schrefler. A multifrontal parallel algorithm for coupled thermo-hydro-mechanical analysis of deforming porous media. *Int. J. Numer. Methods. Eng.* 43:1069–1083, 1998.
 - ⁴⁵Zienkiewicz, O. C. Coupled problems & their numerical solution. In: *Numerical Methods in Coupled Systems*, edited by R. W. Lewis, P. Bettes, and E. Hinton. Chichester: Wiley, pp. 35–58, 1984.
 - ⁴⁶Zienkiewicz, O. C., D. K. Paul, and A. H. C. Chan. Unconditionally stable staggered solution procedure for

- soil-pore fluid interaction problems. *Int. J. Numer. Methods Eng.* 26:1039–1055, 1988.
- ⁴⁷Zieske, J. D., S. C. Higashij, S. J. Spurmic, and I. K. Gipson. Biosynthetic response of the rabbit cornea to a keratectomy wound. *Invest. Ophthalmol. Vis. Sci.* 28:1668–1677, 1987.
- ⁴⁸Zohdi, T. I. An adaptive-recursive staggering strategy for simulating multifield coupled processes in microheterogeneous solids. *Int. J. Numer. Methods Eng.* 53:1511–1532, 2002.
- ⁴⁹Zohdi, T. I. Modeling and simulation of a class of coupled thermo-chemo-mechanical processes in multiphase solids. *Comput. Methods Appl. Mech. Eng.* 193/6-8:679–699, 2004.
- ⁵⁰Zohdi, T. I. (2010). Simulation of coupled microscale multiphysical-fields in particulate-doped dielectrics with staggered adaptive FDTD. *Comput. Methods Appl. Mech. Eng.* 199:79–101, 2010.
- ⁵¹Zohdi, T. I., and P. Wriggers. Introduction to Computational Micromechanics. Springer-Verlag, 2008.